ISSN 0016-7029, Geochemistry International, 2021, Vol. 59, No. 8, pp. 743–756. © Pleiades Publishing, Ltd., 2021.
Russian Text © The Author(s), 2021, published in Geokhimiya, 2021, Vol. 66, No. 8, pp. 694–708.

Evolution of the Lithospheric Mantle beneath the Nakyn Kimberlite Field: Evidence from Garnets in the Peridotite Xenoliths of the Nyurba and Botuoba Pipes

A. L. Ragozin[a, b, *], A. M. Agashev[a], D. A. Zedgenizov[a, b], and A. A. Denisenko[a]

[a] *Sobolev Institute of Geology and Mineralogy, Siberian Branch, Russian Academy of Sciences, Novosibirsk, 630090 Russia*
[b] *Novosibirsk State University, Novosibirsk, 630090 Russia*
**e-mail: ragoz@igm.nsc.ru*

Received October 7, 2020; revised December 11, 2020; accepted January 3, 2021

Abstract—The paper presents data on garnets from serpentinized peridotite xenoliths in the Nyurba and Botuoba kimberlite pipes of the Nakyn kimberlite field. The major and trace-element compositions of the garnets were analyzed to determine their compositional specifics and genesis. Based on the REE content and chondrite-normalized distribution patterns, the garnets are divided into two types with sinusoidal ($(Sm/Er)_n > 1$) and normal ($(Sm/Er)_n < 1$) REE distribution patterns. In terms of the Y, Zr, Ti, and Eu relations, and the shape of REE distribution pattern, all the garnets correspond to garnets of metasomatized peridotites, except for one sample falling into the field of depleted garnets of harzburgite–dunite paragenesis. The geochemical characteristics of the garnets record two types of metasomatic agents: carbonatite/fluid for type 1 garnets and silicate/melt for type 2 garnets. The carbonatite metasomatic agent produced harzburgitic garnet and its further transformation into lherzolitic garnet. Silicate metasomatism, which led to the formation of the REE pattern of type 2 garnets, likely overprinted two different types of garnets and, respectively, gave two evolutionary trends. These are depleted residual garnets and type 1 garnets previously subjected to carbonatite metasomatism. The low Y and Th contents in combination with the low Ti/Eu ratios in garnets suggest a moderate reworking of lithospheric peridotites by silicate melts, which is consistent with the high diamond grade of the Nakyn kimberlite field.

Keywords: garnet, peridotite, upper mantle, REE, Siberian craton, mantle metasomatism
DOI: 10.1134/S0016702921080061

INTRODUCTION

Lithospheric mantle beneath Archean continental blocks (cratons) extends to a depth approximately 220–250 km (Rudnick and Nyblade, 1999; Eaton et al., 2009) and consists mainly of ultramafic rocks and less abundant eclogites and pyroxenites (Sobolev, 1974). These rocks are available for study only as xenoliths brought to the surface by kimberlites, lamproites, and sometimes by other deep-seated magmas (lamprophyric or alkali basaltic ones). Kimberlites are high-K and low-Na olivine-rich (~50 mod %) ultramafic rocks with high CO_2 and H_2O content, which are formed through partial melting at depths over 200 km (Pearson et al., 2019). They are complex hybrid rocks containing numerous mantle fragments, first of all, olivine with scarce diamonds embedded in a magmatic matrix (Mitchel et al., 2019). Mantle xenoliths in kimberlite pipes provide insight into the deepest seated horizons of lithospheric mantle. Peridotite xenoliths bearing clear evidence for mantle metasomatism were found in kimberlites worldwide (e.g., Pearson et al., 2003; Bell et al., 2005; Grégoire et al., 2008; Arndt et al., 2009; Agashev et al., 2013; Howarth et al., 2014; Pokhilenko et al., 2015).

The lithospheric mantle beneath the Siberian craton is well studied in the Udachnaya pipe area owing to the abundance of large and very fresh, practically unaltered xenoliths (Shatsky et al., 2008; Ionov et al., 2010, 2017; Doucet et al., 2012; Agashev et al., 2013; Howarth et al., 2014). The study of garnet from peridotites of the Udachnaya pipe allowed Pokhilenko et al. (2015) to propose a generalized model of metasomatic evolution of lithospheric peridotites of the Siberian Craton and to determine the compositions of metasomatic agents, main metasomatic stages, and their succession.

In 1990, the diamondiferous Nyurba and Botuoba pipes were discovered in the Nakyn kimberlite field in the central part of the Markha terrane, the Anabar tectonic province (Fig. 1). The Markha dike and Maiskoe body were found in the vicinity of these pipes (Tolstov et al., 2009). The kimberlites of the Nyurba and Botuoba pipes define the Rb–Sr isochron ages of 364 ± 5 and 364 ± 9 Ma, respectively (Agashev et al., 2001; 2004). Geological data con-

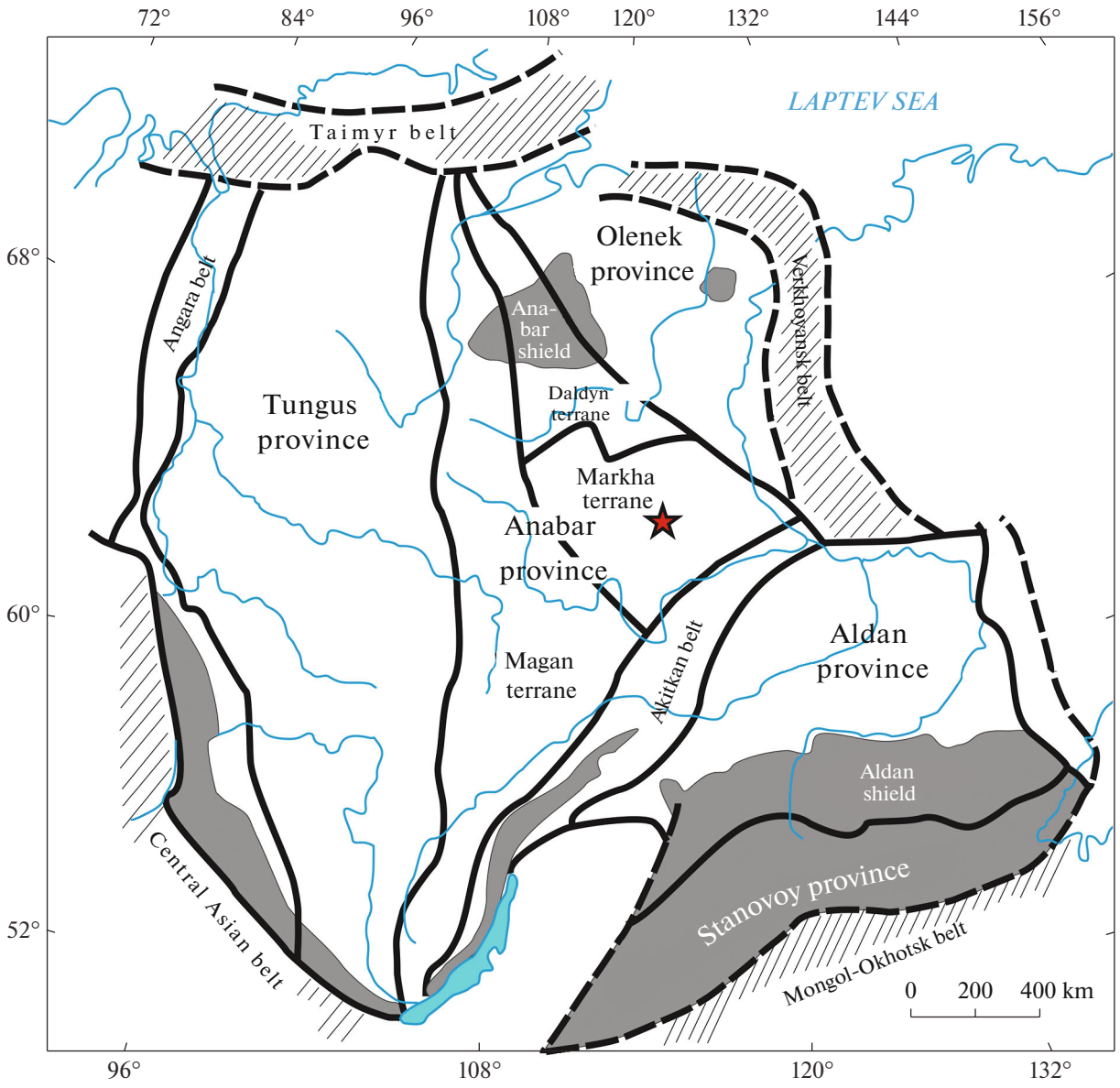

Fig. 1. Tectonic scheme of the Siberian platform basement after (Rosen et al., 2006; Koreshkova et al., 2011). Gray color shows the exposed Precambrian basement, white fields are post-Riphean sedimentary cover, diagonal shading designates Phanerozoic mobile belts. Asterisk shows the Nakyn kimberlite field.

strain the emplacement age of the Nyurba pipe within 384–374 Ma (Kiselev et al., 2014). Both these determinations correspond to the middle Paleozoic episode of diamondiferous pipe formation at the Siberian Craton (Sun et al., 2014; Agashev et al., 2020). In terms of some mineralogical and geochemical features, kimberlites of the Nakyn field are close to group II kimberlites (micaceous orangeites) of South Africa (Agashev et al., 2001; Pokhilenko et al., 2000). Only few data are available on mantle xenoliths from kimberlites of the Nakyn field. Diamond-bearing microxenoliths found in the kimberlites of the Nyurba pipe frequently represent garnet intergrowths with diamonds (Spetsius et al., 2008; Malkovets et al., 2008). Based on the chemical composition, the majority of garnets are ascribed to eclogitic or pyroxenitic parageneses, with subordinate harzburgitic and lherzolite–wehrlitic garnets. Wide oxygen isotope variations in the eclogitic garnets point to their subduction origin together with diamonds (Spetsius et al., 2008). The peridotitic garnets are most resistant to secondary alterations and their relicts could be used to decipher the composition and metasomatic reworking of lithospheric mantle (Griffin et al., 1999a). New major and trace element data on garnets from the peridotite xenoliths in the Nyurba and Botuoba kimblerite pipes reported in this work were used to determine the composition and genesis of mantle protoliths of this region.

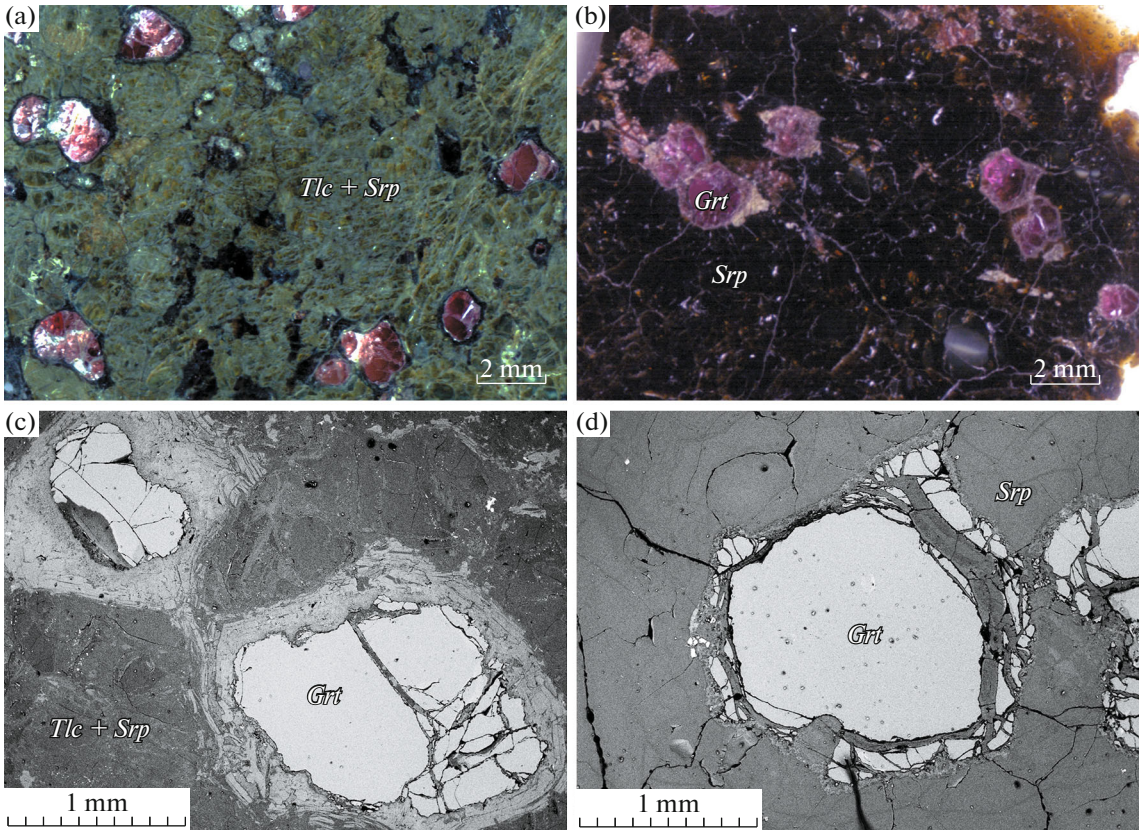

Fig. 2. Relations of garnets with products of secondary replacement in peridotite xenoliths ((a–b) transmitted light, (c–d) BSE image; (*Grt*) garnet; (*Tlc*) talc, (*Srp*) serpentine).

SAMPLES AND METHODS

The studied collection includes 37 peridotite xenoliths from the Nyurba (12 samples) and Botuoba (25 samples) kimberlite pipes. The xenoliths usually have ellipsoid shape up to 8 cm long. They were subjected to strong secondary alterations and were practically completely serpentinized. The preserved mantle minerals are only garnet and scarce globules of accessory sulfides. Garnet from 0.5 to 8 mm in size usually has equant rounded shape and retained crystallographic faceting. Kelyphitic (reaction) rims amounting up to 10 vol % are developed around most of extracted grains and along cross-cutting fractures (Fig. 2)

The xenoliths yielded 181 grains of red-lilac or pink-violet garnets. Their major-element composition was analyzed on an X-ray Jeol JXA-8100 microprobe at the Sobolev Institute of Geology and Mineralogy of the Siberian Branch of the Russian Academy of Sciences at an accelerating voltage of 15 kV and a beam current of 20 nA. Natural minerals and synthetic grains were used as standards. The measurement technique is described in detail in (Lavrentiev et al., 2015).

The trace-element composition of the garnets was analyzed by mass spectrometric method using a XSERIES2 (Thermo Scientific) quadrupole inductively coupled plasma mass spectrometer coupled with a laser sampler with a wave length of 213 nm (New Wave Research, Nd:YAG solid state laser) at the Novosibirsk State University. Multielement certified standard samples of NIST 612 50 ppm glass standard and NIST 614 1 ppm glass standard were used as external standards. The Ca concentrations determined using X-ray microanalysis were used as an internal standard. The NIST 610 reference material was measured to perform instrumental drift correction. The mass spectrometer parameters involved ion lens stack voltage, reference mass calibration, and other parameters, which provided the maximum sensitivity within a full range of analyzed masses, and were optimized using 10 mg/L Mg, In, Ce, Ba, and U solution in 0.5% HNO_3. The nebulizer gas flow was adjusted so that the CeO/Ce and Ba^{2+}/Ba^{+} were less than 3%. The element concentrations in a "dry" aerosol obtained on laser sampler were measured in a peak jumping mode. The elements were measured in a resolution mode with a peak width of 0.7 amu, and the peak intensity for each studied element was measured as the signal intensity in the central part of mass range determined for each element. The quadrupole delay time was 10 ms per each mass, with a one scan over all masses. Counting time was 90 s per point, including 30 s for determination of background values. The signal was measured simulta-

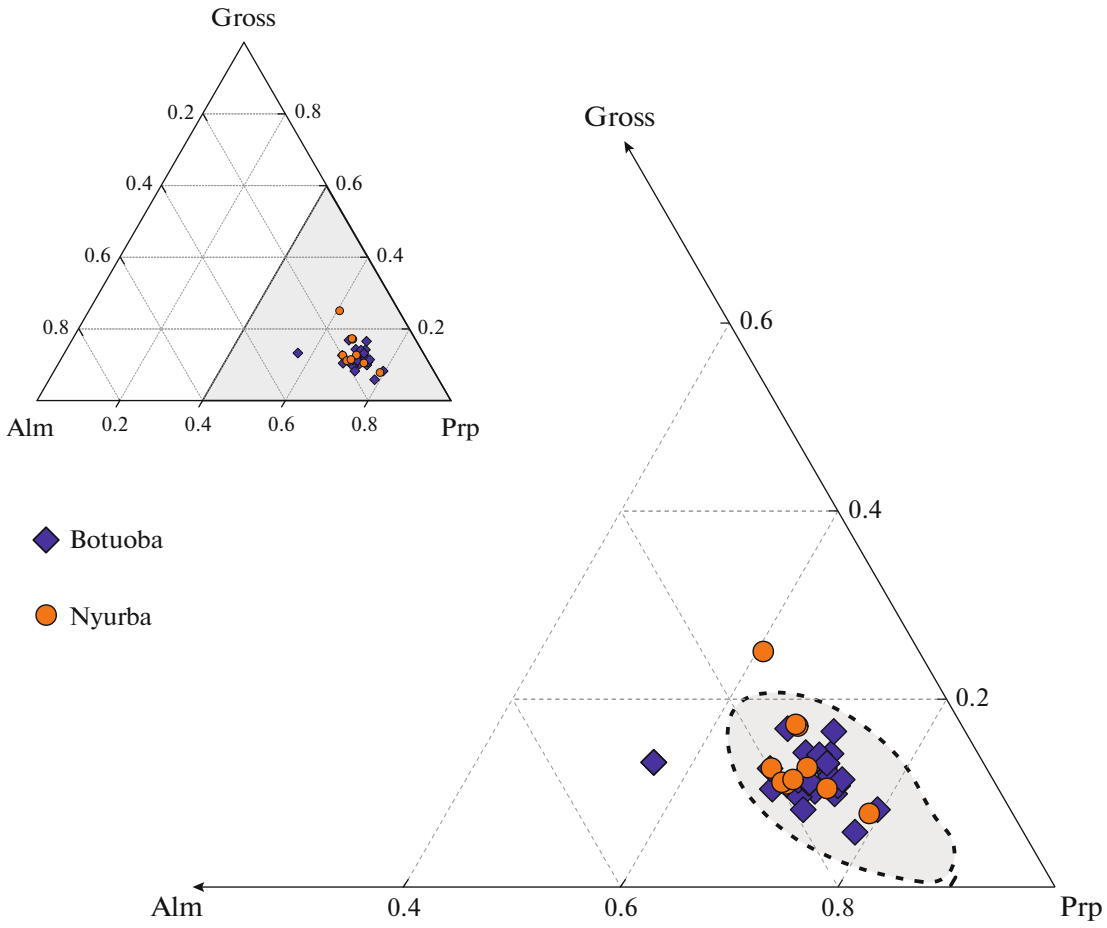

Fig. 3. Compositions of garnets from peridotite xenoliths in the kimberlites of the Nkyn field in the pyrope–almandine–grossular diagram. Gray color shows the field of garnet inclusions of ultrabasic paragenesis in diamonds from kimberlites of the Siberian Platform (Taylor and Anand, 2004).

neously in pulsed (calculation of amount falling on ion detector) and analog modes. Data were acquired using time resolved analysis (TRA) as "time sections" in order to determine the element variations with time. Analyzed isotopes were determined simultaneously by mass and time required to attain maximum in a "time section". The NIST 612 standards were analyzed each ten samples.

RESULTS

Major-Element Composition of Garnets

The major-element composition of the studied garnets from xenoliths shows wide variations (Table 1). In some xenoliths and within individual grains, garnet composition has no significant differences. The garnets contain from 58 to 85 mol % pyrope (Prp), from 6 to 25 mol % grossular (Gross), and from 12 to 20 mol % almandine (Alm) (Fig. 3). In terms of proportions of these components, the majority of the garnets fall in the compositional field of garnets from peridotite xenoliths from many other kimberlite deposits of the Siberian platform, in particular, from the Udachnaya pipe (Taylor and Anand, 2004).

All the studied garnets have high magnesian number (Mg# 76-87) and the low contents of TiO_2 (<0.46 wt %) and MnO (0.26–0.54 wt %). The CaO content varies within 2.3–6.3 wt %, except for garnet from sample AH-3/16ko with 9.8 wt % CaO. The Cr_2O_3 content varies from 0.7 to 11.2 wt %. Most of the studied garnets (garnets from 41 samples) demonstrate a positive CaO–Cr_2O_3 correlation typical of lherzolitic garnets (Fig. 4). A change of garnet composition with decreasing CaO and Cr_2O_3 along a lherzolitic trend reflects a clinopyroxene control (Griffin et al., 1999a; Kopylova et al., 2000). Garnets from six samples correspond to harzburgite–dunite paragenesis, but only one of them (AH8/16-3) is ascribed to the diamondiferous assemblage according to (Sobolev et al., 1973). Only one xenolith (AH3/16ko) can be ascribed to pyroxenites. Garnet in this sample has high CaO content, which in combination with low Cr_2O_3 content is typical of a websteritic paragenesis.

Table 1. Major element composition (wt %) of garnets in peridotite xenoliths from the kimberlites of the Nakyn field

Sample	*n*	SiO_2	TiO_2	Al_2O_3	Cr_2O_3	FeO	MnO	MgO	CaO	Na_2O	Total
Bt1/16	2	40.2	0.094	16.4	8.58	7.81	0.351	18.1	6.34	0.044	97.9
σ		0.1	0.007	0.0	0.03	0.02	0.004	0.0	0.01	0.002	0.05
Bt2/16	9	43.0	0.114	22.8	0.83	7.73	0.421	21.1	3.89	0.038	99.9
σ		0.1	0.008	0.3	0.11	0.03	0.008	0.1	0.02	0.022	0.3
Bt2/16ko	1	42.8	0.101	22.0	1.67	8.90	0.478	19.8	4.31	0.023	100.1
Bt6/16ko	3	41.7	0.167	17.9	7.15	6.67	0.332	20.0	5.46	0.059	99.3
σ		0.5	0.020	0.3	0.25	0.06	0.040	0.1	0.13	0.005	0.8
Bt6/16	8	41.8	0.165	22.2	1.39	8.68	0.464	20.8	4.05	0.056	99.6
σ		0.1	0.031	0.1	0.10	0.23	0.018	0.2	0.11	0.019	0.1
Bt8/16	5	41.4	0.399	17.8	6.85	5.90	0.286	19.5	6.28	0.082	98.4
σ		0.2	0.016	0.2	0.09	0.04	0.004	0.1	0.03	0.008	0.4
Bt10/16	1	41.3	0.254	21.7	1.50	9.79	0.479	19.9	4.33	0.083	99.3
Bt10/16ko	1	41.3	0.129	19.2	4.90	7.61	0.404	20.7	5.03	0.023	99.3
Bt10/16-1	1	41.6	0.234	22.4	0.86	9.63	0.442	20.6	3.84	0.093	99.8
Bt10/16-2	8	41.4	0.244	22.2	0.88	10.61	0.443	19.6	4.14	0.076	99.7
σ		0.1	0.026	0.1	0.05	0.08	0.014	0.1	0.08	0.014	0.1
Bt10/16-2ko	4	41.3	0.059	20.9	3.19	9.07	0.541	20.0	4.46	0.038	99.5
σ		0.1	0.014	0.2	0.15	0.13	0.010	0.2	0.04	0.019	0.2
Bt10/16/A-1ko	1	42.7	0.435	20.6	3.07	7.33	0.376	20.9	4.22	0.102	99.8
Bt11/16	5	41.5	0.240	17.3	7.33	7.08	0.296	19.9	5.01	0.053	98.8
σ		0.4	0.013	0.1	0.07	0.05	0.005	0.1	0.05	0.004	0.1
Bt11/16ko	1	41.3	0.068	20.1	3.94	9.70	0.483	18.4	4.79	0.033	98.8
Bt11/16-2	2	42.1	0.222	21.1	2.23	7.95	0.439	19.7	5.60	0.079	99.4
σ		0.1	0.003	0.2	0.28	0.01	0.015	0.2	0.11	0.004	0.1
Bt11/16-2ko	2	42.2	0.214	21.6	1.63	7.80	0.418	20.1	5.23	0.066	99.2
σ		0.0	0.009	0.0	0.01	0.01	0.005	0.0	0.05	0.005	0.05
Bt11/16-3	4	42.6	0.053	21.7	2.60	6.17	0.281	22.5	3.23	0.038	99.2
σ		0.2	0.009	0.2	0.11	0.14	0.002	0.1	0.03	0.002	0.6
Bt12/16	4	41.0	0.423	17.9	6.33	7.19	0.314	19.6	5.38	0.098	98.3
σ		0.4	0.007	0.1	0.12	0.06	0.006	0.0	0.05	0.014	0.6
Bt12/16-1	1	41.6	0.074	20.0	4.40	8.43	0.403	19.8	4.23	0.039	98.9
Bt13/16-1	3	41.2	0.179	20.9	2.92	7.48	0.349	20.2	4.68	0.072	98.0
σ		0.4	0.043	0.4	0.24	0.06	0.012	0.2	0.04	0.005	0.7
Bt13/16-2	3	42.0	0.032	20.4	4.24	7.73	0.379	22.0	2.27	0.041	99.1
σ		0.1	0.006	0.1	0.28	0.01	0.006	0.1	0.09	0.010	0.3
Bt13/16-4ko	1	42.1	0.458	19.7	3.72	7.01	0.379	21.1	4.49	0.100	99.1
Bt14/16	2	41.8	0.200	19.5	5.00	7.11	0.319	20.0	5.06	0.079	99.0
σ		0.0	0.130	1.9	2.79	0.30	0.041	0.2	0.33	0.009	1.2
Bt15/16	8	41.6	0.072	20.8	3.36	8.42	0.419	19.9	4.31	0.039	98.9

Table 1. (Contd.)

Sample	*n*	SiO_2	TiO_2	Al_2O_3	Cr_2O_3	FeO	MnO	MgO	CaO	Na_2O	Total
σ		0.2	0.007	0.2	0.12	0.15	0.013	0.2	0.03	0.004	0.4
Bt-quarry	2	41.3	0.172	20.4	3.32	9.63	0.526	20.6	3.23	0.086	99.3
σ		0.1	0.005	0.4	0.04	0.03	0.014	0.1	0.02	0.012	0.2
AH2/16	29	41.7	0.217	21.8	1.46	9.76	0.467	19.8	4.32	0.058	99.5
σ		0.6	0.026	0.1	0.05	0.07	0.008	0.2	0.04	0.014	0.3
AH3/16ko	1	41.9	0.056	21.4	1.61	7.21	0.259	17.1	9.84	0.015	99.5
AH7/16	19	41.6	0.050	20.8	3.24	9.09	0.431	19.3	4.27	0.040	98.8
σ		0.2	0.010	0.2	0.16	0.22	0.024	0.2	0.05	0.005	0.3
AH8/16-1	5	41.3	0.209	19.1	5.11	8.12	0.330	19.6	4.89	0.050	98.6
σ		0.1	0.010	0.1	0.01	0.03	0.010	0.1	0.02	0.011	0.2
AH8/16-2	7	41.2	0.043	20.3	3.77	9.66	0.487	18.5	4.82	0.030	98.8
σ		0.4	0.009	0.3	0.20	0.14	0.014	0.2	0.13	0.009	0.7
σ		0.1	0.009	0.3	0.43	0.13	0.005	0.1	0.08	0.009	0.5
AH9/16	2	40.1	0.196	14.4	11.11	7.28	0.345	18.3	6.42	0.058	98.2
σ		0.2	0.008	0.0	0.13	0.02	0.012	0.0	0.06	0.008	0.4
AH10/16	3	42.4	0.211	22.1	1.51	9.78	0.478	19.4	4.33	0.042	100.2
σ		0.2	0.019	0.2	0.01	0.05	0.009	0.0	0.02	0.015	0.2
AH11/16	2	40.4	0.193	14.4	11.10	7.33	0.328	18.2	6.50	0.063	98.5
σ		0.0	0.011	0.0	0.06	0.04	0.002	0.0	0.10	0.006	0.05
AH20/16	22	41.5	0.061	21.4	2.61	8.02	0.461	21.0	4.15	0.038	99.3
σ		0.1	0.009	0.2	0.18	0.21	0.017	0.2	0.04	0.013	0.2
AH24/16ko	1	42.4	0.060	20.8	3.16	9.08	0.538	19.4	4.40	0.042	99.9

n is the number of analyzed garnets, σ is the standard deviation; (Bt) Botuoba pipe, (AN) Nyurba pipe.

Trace Element Composition of Garnets

The studied garnets from peridotite xenoliths in the kimberlites of the Nakyn Field have wide variations of trace and rare-earth (REE) elements (Table 2). The trace and REE contents were analyzed in the core and rims of each garnet grains in each sample. No significant variations were found both within garnet grain and within most samples. In terms of REE contents and chondrite-normalized (McDonough and Sun, 1995) distribution patterns, they can be divided into two types.

The type 1 garnet has a sinusoidal pattern (Fig. 5a) with $(Sm/Er)_n > 1$ (*n*—normalized to chondrite composition) and $(Nd/Er)_n > 1$ for garnet from sample Bt-12/16-1. In terms of major e-element composition, these garnets are ascribed to the lherzolitic and harzburgitic parageneses. Their patterns are characterized by LREE and MREE enrichment, which widely varies in different samples. The sinusoidal distribution is best expressed in the harzburgitic garnet from sample Bt13/16-2 $(Sm/Er)_n = 40.3$ and $(La/Yb)_n = 0.4$) and least expressed in high-Cr lherzolitic garnets from samples Bt13/16-1 and Bt14/16 ($(Sm/Er)_n = 1.16–1.18$ and $(La/Yb)_n = 0.002–0.004$).

Type 2 garnets are characterized by the LREE depletion and enrichment in MREE and HREE: $(Sm/Er)_n < 1$, $(La/Yb)_n = 0.001–0.008$. (Fig. 4b). Thereby, such garnets are characterized by a flat MREE and HREE patterns ($(Yb/Sm)_n < 5$). In terms of CaO and Cr_2O_3 contents, most garnets of this group correspond to lherzolitic paragenesis. The same REE distribution is also typical of websteritic garnet with high CaO content. Garnets in association with diamond are characterized by sinusoidal REE pattern (Shchukina et al., 2017), but harzburgitic garnet from sample An 8/16-3 shows the normal REE distribution at relatively low MREE and HREE contents.

Two samples have atypical REE patterns (Fig. 5b). Garnet from sample Bt10/16ko has fractionated REE pattern with successive increase of normalized ratios ($(La/Yb)_n = 0.005$ and $(Yb/Sm)_n = 13.4$). Garnet from

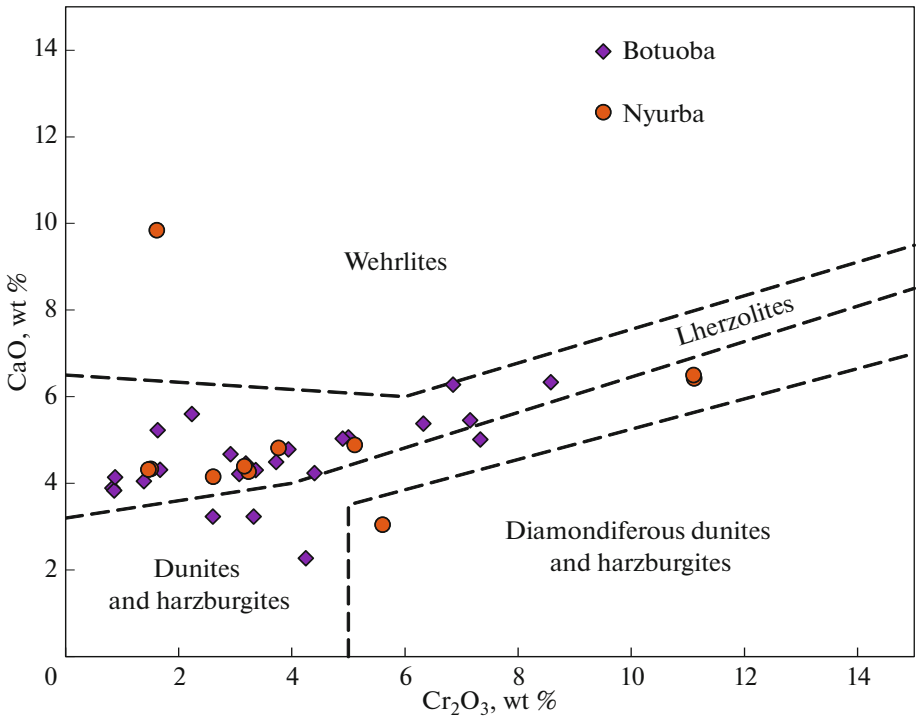

Fig. 4. Garnets in peridotites from kimberlites of the Nakyn field in the Cr_2O_3–CaO diagram (Sobolev et al., 1973).

sample Bt 1/16 has low REE contents typical of garnets formed by exsolution of garnet from high-temperature orthopyroxene (Shchukina et al., 2017).

DISCUSSION

Kimberlites of the Nakyn field differ from known kimberlites from other fields of the Siberian Platform (Tomshin et al., 1998; Agashev et al., 2001; Kornilova et al., 2001; Spetsius et al., 2006; Konstantinov et al., 2017) in the high content of phlogopite, low contents of incompatible elements compared to typical kimberlites, and have Sr and Nd isotope composition transitional between group-I kimberlites and orangeites (group II kimberlites). These differences could be related to the lateral mantle heterogeneity and metasomatic process, which caused geochemical reworking of upper mantle of the corresponding region. Mantle metasomatism was caused by diverse mantle fluids/melts (Andersen and Neumann 2001; Klein-Ben-David et al., 2004; Tomlinson et al., 2006; Bussweiler et al., 2018; Zedgenizov et al., 2020). It is expressed in peculiar trace-element and rare-earth element distribution in clinopyroxenes and garnets (Hoal et al., 1994; Griffin et al., 1999b; Agashev et al., 2013; Pokhilenko et al., 2015; Shchukina et al., 2017; Shchukina et al., 2019). Two types of metasomatic agents affected the lithospheric mantle: silicate melts and carbonatite melts/fluids. There are different points of view concerning the composition of the silicate metasomatic agent. Some researchers suggest that it was silicate melt close to picrite in terms of trace-element composition (Shchukina et al., 2017; Agashev, 2019), while others believe that it was close to host kimberlite (Kargin et al., 2017) or protokimberlite melt corresponding in composition to the early kimberlite portion crystallized in mantle (Bussweiler et al., 2018). It was proposed in the latter case that xenoliths from kimberlites bear information only on the mantle channel, in which the early portions of kimberlite melt were solidified, and do not reflect the structure of the entire lithospheric mantle. However, this hypothesis seems to be ambiguous, since exotic mantle xenoliths such as ilmenite peridotites, wehrlites, strongly metasomatized sheared peridotites, and, especially scarce MARID (Mica–Amphibole–Rutile–Ilmenite–Diopside) and PIC (Phlogopite–Ilmenite–Clinopyroxene) rocks in combination account for no more than 10% of all kimberlite xenoliths (Sobolev, 1974). In addition, it is reasonable to expect in this case that xenoliths represent the infill of this channel, i.e., failed kimberlite.

It was believed for a long time that one of the main evidences for metasomatic alteration of lithospheric mantle is the presence of phlogopite in mantle peridotites (Carswell 1980; Grégoire et al., 2003; Harte, 1983; Hawkesworth et al., 1990; Kopylova et al., 1999). So-called “phlogopite” metasomatism occurred in mantle at relatively low temperatures ($T < 1100$°C), as was exemplified by peridotites from the Wesselton pipe, South Africa (Griffin et al., 1999b). However, the study of the unaltered peridotite xenoliths from the Udachnaya pipe (Agashev et al., 2013; Doucet et al.,

Table 2. Trace-element composition (ppm) of garnets in peridotite xenoliths from the kimberlites of the Nakyn field

Sample	*n*	Cs	Rb	Ba	Th	U	Nb	Ta	La	Ce	Pr	Sr	Nd	Zr	Hf	Sm	Eu	Ti	Gd	Tb	Dy	Y	Ho	Er	Tm	Yb	Lu
Bt1/16	2	bdl	bdl	0.004	0.028	0.011	0.079	0.008	0.036	0.330	0.081	1.007	0.547	4.358	0.114	0.190	0.091	588	0.320	0.051	0.362	1.993	0.077	0.239	0.048	0.358	0.086
σ				0.004	0.003	0.001	0.012	0.003	0.005	0.007	0.010	0.020	0.026	0.089	0.004	0.001	0.005	1	0.007	0.003	0.036	0.005	0.001	0.020	0.000	0.056	0.001
Bt 2/16	9	bdl	0.088	0.236	0.040	0.001	0.001	bdl	0.003	0.043	0.027	0.064	0.452	11.64	0.214	0.618	0.353	726	1.638	0.368	3.060	18.65	0.722	2.357	0.386	2.965	0.482
σ			0.012	0.003	0.001	0.001	0.001	0.043	0.001	0.005	0.003	0.042	0.048	1.341	0.041	0.052	0.025	49	0.021	0.116	0.024	0.012	0.243	0.059	0.231	0.040	0.254
Bt 2/16ko	1	bdl	0.043	0.002	0.004	0.004	0.011	0.001	0.014	0.143	0.069	0.079	1.076	10.04	0.128	1.173	0.536	458	2.461	0.514	4.114	23.90	0.899	2.657	0.358	2.386	0.329
Bt 6/16ko	2	bdl	0.098	0.047	0.031	0.039	0.149	0.021	0.051	0.580	0.220	0.635	1.900	11.85	0.345	0.829	0.305	1121	1.002	0.155	1.121	6.045	0.230	0.678	0.101	0.811	0.145
σ				0.030	0.009	0.014	0.347	0.009	0.011	0.095	0.033	0.010	0.026	0.865	0.010	0.059	0.015	44	0.034	0.060	0.004	0.097	0.021	0.005	0.010	0.005	0.019
Bt 6/16	8	bdl	bdl	0.014	0.016	0.016	0.183	0.018	0.026	0.371	0.195	0.801	2.116	17.79	0.503	1.192	0.413	1006	1.379	0.207	1.519	8.148	0.316	0.892	0.138	0.961	0.169
σ				0.007	0.004	0.008	3.014	0.050	3.180	1.977	0.055	0.056	0.131	1.515	0.037	0.044	0.021	294	0.022	0.079	0.013	2.186	0.082	0.023	0.096	0.021	0.196
Bt 8/16	3	0.029	0.024	0.004	0.004	0.010	0.084	0.016	0.015	0.208	0.105	0.505	1.192	59.67	1.711	0.761	0.360	2688	1.957	0.449	3.668	19.62	0.767	2.075	0.299	1.916	0.298
σ		0.006	0.033	0.003	0.002	0.003	0.001	0.002	0.006	0.047	0.015	0.095	0.086	0.754	0.046	0.056	0.015	34	0.024	0.017	0.015	0.165	0.007	0.040	0.006	0.076	0.010
Bt 10/16	1	bdl	0.038	bdl	0.005	0.012	0.422	0.043	0.009	0.154	0.073	0.175	0.730	59.34	0.645	0.543	0.308	1070	1.753	0.417	3.580	20.76	0.807	2.201	0.301	1.890	0.270
Bt 10/16ko	1	bdl	0.038	0.011	0.021	0.028	0.049	0.002	0.032	0.233	0.065	0.252	0.499	6.117	0.118	0.299	0.165	3018	0.858	0.279	3.229	23.77	0.934	3.415	0.581	4.359	0.687
Bt 10/16-1	1	bdl	0.016	0.000	0.005	0.007	0.004	0.000	0.004	0.043	0.032	0.063	0.473	31.95	0.424	0.657	0.421	1577	1.882	0.429	3.628	21.88	0.846	2.454	0.355	2.352	0.350
Bt 10/16-2	8	bdl	0.031	0.048	0.044	0.032	0.023	0.002	0.044	0.089	0.025	0.170	0.433	20.23	0.336	0.832	0.469	1823	2.153	0.485	4.251	26.90	1.040	3.337	0.507	3.669	0.548
σ			0.015	0.006	0.111	0.057	0.779	0.020	0.116	0.149	0.009	0.064	0.022	0.769	0.015	0.025	0.012	103	0.011	0.085	0.016	0.327	0.164	0.030	0.086	0.015	0.069
Bt 10/16-2ko	4	bdl	0.065	0.002	0.015	0.027	0.014	0.002	0.025	0.245	0.089	0.164	1.032	7.789	0.089	1.016	0.494	417	2.172	0.454	3.447	18.77	0.728	2.180	0.320	2.258	0.355
σ			0.012	0.002	0.007	0.020	2.026	0.035	0.015	0.103	0.032	0.040	0.338	0.677	0.039	0.204	0.029	81	0.038	0.049	0.020	0.060	0.165	0.044	0.116	0.016	0.122
Bt 10/16/A-1ko	1	bdl	0.131	0.002	0.009	0.018	0.148	0.022	0.009	0.109	0.041	0.153	0.530	23.72	0.661	0.623	0.342	2542	1.916	0.448	3.907	22.15	0.927	2.871	0.439	3.259	0.525
Bt11/16	2	bdl	bdl	0.666	0.030	0.065	0.485	0.046	0.053	0.663	0.262	0.978	2.524	22.21	0.540	1.268	0.451	1632	1.631	0.244	1.647	8.752	0.332	0.947	0.140	1.091	0.201
σ				0.027	0.008	0.013	0.315	0.008	0.010	0.086	0.030	0.009	0.024	0.787	0.009	0.054	0.014	40	0.030	0.055	0.003	0.088	0.019	0.004	0.009	0.005	0.018
Bt11/16ko	1	0.093	0.762	0.907	0.036	0.084	0.990	0.045	0.236	0.870	0.246	11.09	1.924	18.06	0.433	0.892	0.317	1166	1.112	0.179	1.112	6.345	0.226	0.642	0.107	0.796	0.131
Bt 11/16-2	2	bdl	bdl	0.395	0.131	0.030	0.020	0.001	0.422	0.572	0.091	3.450	0.934	21.91	0.462	0.892	0.399	1556	1.584	0.323	2.786	17.70	0.685	2.305	0.359	2.713	0.424
σ				0.022	0.007	0.011	0.262	0.007	0.008	0.072	0.025	0.008	0.020	0.653	0.007	0.045	0.012	33	0.025	0.045	0.003	0.073	0.016	0.004	0.007	0.004	0.015
Bt 11/16-2ko	2	bdl	0.171	1.156	0.014	0.015	0.022	0.001	0.365	0.696	0.111	14.77	0.906	12.45	0.252	0.724	0.326	979	1.160	0.227	1.826	11.31	0.425	1.391	0.221	1.645	0.257
σ			0.094	0.019	0.006	0.009	0.225	0.006	0.007	0.062	0.022	0.006	0.017	0.562	0.006	0.039	0.010	28	0.022	0.039	0.002	0.063	0.014	0.003	0.006	0.003	0.013
σ		0.067	0.020	0.002	0.001	0.001	0.001	0.002	0.001	0.008	0.006	0.012	0.081	0.996	0.029	0.069	0.017	11	0.070	0.004	0.042	0.135	0.002	0.041	0.007	0.045	0.005
Bt12/16	3	bdl	bdl	0.003	0.014	0.022	0.227	0.055	0.035	0.532	0.202	0.803	1.758	35.93	0.951	1.058	0.425	2910	1.941	0.387	3.096	18.96	0.686	2.236	0.318	2.163	0.345
σ				0.001	0.006	0.005	0.034	0.003	0.012	0.040	0.018	0.041	0.065	0.756	0.047	0.040	0.024	94	0.088	0.024	0.096	0.273	0.020	0.099	0.013	0.015	0.014
Bt12/16-1	1	bdl	bdl	0.003	0.006	0.016	0.026	0.002	0.015	0.240	0.156	0.137	1.642	5.289	0.120	0.373	0.117	432	0.225	0.044	0.335	3.490	0.110	0.521	0.126	1.138	0.244
Bt13/16-1	3	0.006	0.044	0.003	0.009	0.010	0.008	0.001	0.006	0.120	0.089	0.160	1.369	34.27	0.760	1.285	0.621	1278	2.714	0.501	3.019	13.69	0.507	1.200	0.159	1.173	0.217
σ		0.003	0.016	0.003	0.006	0.007	0.003	0.001	0.003	0.077	0.038	0.110	0.337	4.936	0.138	0.127	0.036	258	0.218	0.013	0.101	0.349	0.013	0.038	0.003	0.097	0.007
Bt13/16-2	3	0.176	0.114	0.015	0.009	0.227	0.106	0.007	0.165	4.028	2.892	4.481	25.61	14.35	0.313	3.818	0.727	232	1.689	0.105	0.381	1.476	0.052	0.102	0.019	0.289	0.092
σ		0.106	0.021	0.006	0.003	0.013	0.006	0.002	0.015	0.583	0.229	0.253	0.522	0.266	0.014	0.241	0.027	5	0.177	0.010	0.035	0.090	0.010	0.007	0.003	0.019	0.001
Bt 13/16-4ko	1	bdl	bdl	0.016	0.009	0.008	0.042	0.002	0.166	0.479	0.110	0.266	1.168	11.64	0.160	1.128	0.524	613	2.498	0.552	4.746	31.39	1.166	3.934	0.643	4.898	0.783
Bt14/16	1	0.019	bdl	0.005	0.004	0.002	0.002	0.000	0.004	0.035	0.041	0.029	1.067	26.14	0.467	1.367	0.644	813	3.026	0.571	3.313	14.54	0.550	1.253	0.172	1.185	0.228
Bt15/16	3	0.040	0.082	0.001	0.003	0.014	0.024	0.003	0.011	0.161	0.077	0.129	1.296	21.20	0.260	1.390	0.695	527	3.239	0.692	5.026	22.85	0.864	2.405	0.353	2.567	0.441
σ		0.029	0.024	0.000	0.000	0.007	0.008	0.001	0.003	0.078	0.006	0.018	0.044	1.198	0.022	0.061	0.040	27	0.050	0.021	0.106	0.255	0.026	0.049	0.001	0.103	0.032
Bt-quarry	2	bdl	0.011	bdl	0.002	0.005	0.448	0.040	0.001	0.041	0.017	0.063	0.154	108.9	1.057	0.334	0.331	1125	2.601	0.725	6.145	34.48	1.355	3.669	0.463	2.579	0.332
σ			0.052		0.002	0.001	0.018	0.070	0.000	0.000	0.001	0.016	0.018	0.584	0.067	0.027	0.017	49	0.006	0.201	0.008	0.002	0.112	0.053	0.011	0.010	0.001
AH 2/16	3	bdl	0.044	0.003	0.004	0.014	0.008	0.001	0.005	0.074	0.034	0.075	0.455	17.13	0.293	0.586	0.345	1638	1.662	0.386	3.294	20.35	0.773	2.425	0.374	2.737	0.415
σ			0.016	0.003	0.006	0.006	0.003	0.001	0.003	0.075	0.037	0.107	0.329	4.817	0.134	0.124	0.035	112	0.213	0.012	0.099	0.341	0.012	0.037	0.003	0.095	0.007
AH 3/16ko	1	bdl	0.041	0.022	0.002	0.002	0.001	0.003	0.012	0.051	0.037	0.191	0.875	6.059	0.076	1.853	1.025	723	4.977	1.064	8.300	46.16	1.759	5.202	0.758	5.397	0.755
AH7/16	4	0.025	0.023	0.002	0.012	0.009	0.009	0.001	0.019	0.168	0.071	0.144	0.857	7.731	0.072	1.021	0.469	365	2.388	0.513	3.900	21.94	0.844	2.502	0.381	2.638	0.416
σ		0.018	0.039	0.001	0.007	0.003	0.005	0.001	0.008	0.071	0.024	0.018	0.227	1.216	0.027	0.152	0.034	24	0.094	0.042	0.311	1.525	0.064	0.200	0.025	0.100	0.028
AH8/16-1	3	0.094	0.031	0.003	0.002	0.004	0.098	0.022	0.014	0.250	0.111	0.286	1.211	14.74	0.355	0.744	0.271	1426	1.076	0.183	1.420	8.840	0.320	1.068	0.178	1.355	0.249
σ		0.051	0.005	0.000	0.002	0.001	0.007	0.000	0.004	0.008	0.007	0.027	0.067	0.068	0.010	0.065	0.014	11	0.026	0.003	0.084	0.117	0.009	0.021	0.004	0.054	0.017
AH8/16-2	3	0.067	bdl	0.002	0.005	0.000	0.005	0.000	0.005	0.069	0.047	0.082	0.753	3.487	0.068	0.684	0.235	295	0.846	0.126	1.028	8.037	0.289	1.086	0.184	1.625	0.299
σ		0.052	0.042	0.001	0.004	0.000	0.006	0.000	0.001	0.020	0.012	0.016	0.172	0.564	0.024	0.033	0.013	50	0.137	0.019	0.130	0.360	0.027	0.056	0.005	0.048	0.002
AH8/16-3	2	0.072	0.024	0.002	0.001	0.004	0.145	0.019	0.010	0.092	0.039	0.068	0.314	79.23	1.701	0.345	0.188	826	1.076	0.240	1.838	9.217	0.407	1.171	0.173	1.039	0.171
σ		0.026	0.008	0.001	0.001	0.001	0.004	0.001	0.000	0.001	0.008	0.048	0.050	1.919	0.049	0.016	0.005	20	0.043	0.007	0.124	0.722	0.006	0.118	0.022	0.088	0.010
AH9/16	2	0.069	0.042	0.003	0.040	0.032	0.177	0.026	0.053	0.820	0.426	0.737	4.687	50.85	1.252	2.748	0.872	1343	2.519	0.322	1.730	7.295	0.273	0.688	0.099	0.824	0.166
σ		0.093	0.012	0.001	0.037	0.016	0.015	0.008	0.036	0.584	0.254	0.239	1.902	4.503	0.106	0.082	0.126	1	0.307	0.036	0.174	0.464	0.023	0.031	0.007	0.036	0.001
AH 10/16	2	bdl	0.102	bdl	0.006	0.009	0.011	0.001	0.005	0.086	0.041	0.077	0.506	17.44	0.346	0.666	0.368	1692	1.738	0.427	3.548	20.39	0.836	2.625	0.408	2.919	0.454
σ			0.042		0.000	0.005	0.002	0.240	0.013	0.041	0.015	0.003	0.043	2.062	0.086	0.009	0.003	11	0.024	0.004	0.069	0.404	0.004	0.066	0.013	0.049	0.006
AH11/16	3	0.024	bdl	0.003	0.030	0.026	0.200	0.031	0.054	0.696	0.375	0.778	4.554	51.48	1.323	2.758	0.859	1338	2.558	0.311	1.719	7.381	0.283	0.717	0.100	0.794	0.152
σ		0.021	0.015	0.001	0.015	0.012	0.023	0.002	0.037	0.396	0.150	0.148	1.186	2.353	0.047	0.104	0.064	13	0.247	0.021	0.157	0.275	0.006	0.031	0.005	0.018	0.006
AH 20/16	19	bdl	0.068	0.002	0.013	0.014	0.011	0.002	0.019	0.219	0.077	0.145	0.866	16.32	0.170	1.100	0.609	425	2.736	0.533	3.908	21.80	0.841	2.524	0.387	2.869	0.456
σ				0.001	0.004	0.012	0.003	0.032	0.006	0.030	0.009	0.047	0.084	1.369	0.029	0.066	0.027	40	0.029	0.121	0.018	0.033	0.164	0.038	0.128	0.026	0.151
AH 24/16ko	1	bdl	0.080	0.000	0.007	0.008	0.007	0.001	0.011	0.147	0.070	0.118	0.863	6.257	0.046	0.983	0.513	296	2.362	0.494	3.784	20.02	0.814	2.477	0.376	2.689	0.425

(bdl) below detection limit, (n) number of analyzed garnets, (σ) standard deviation; (Bt) Botuoba pipe, (AN) Nyurba pipe.

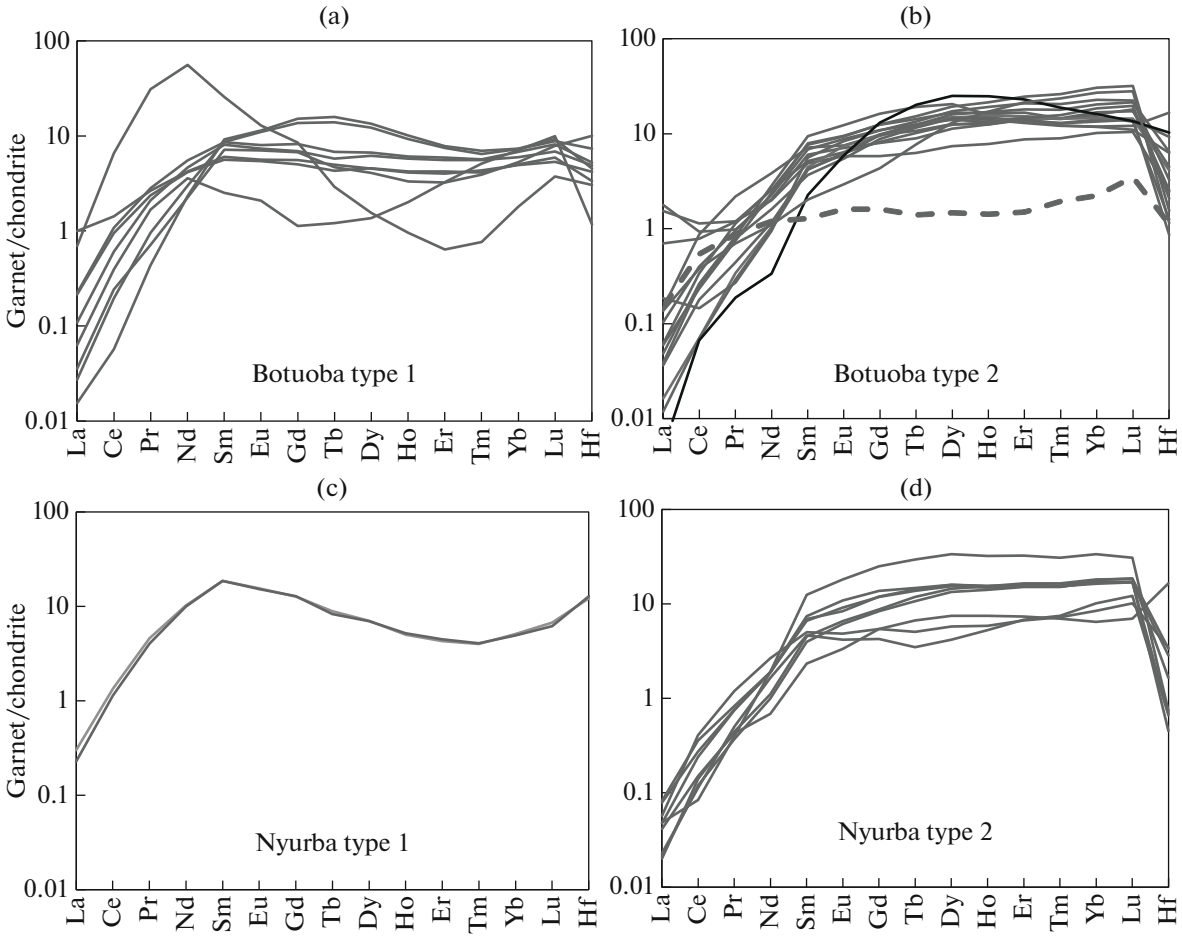

Fig. 5. Types of CI chondrite-normalized (McDonough, Sun, 1995) REE patterns for garnets from peridotites of the Nakyn kimberlite field ((a) Botuoba pipe (type 1), (b) Botuoba pipe (type 2), (c) Nyurba pipe (type 1), (d) Nyurba pipe (type 2). In Fig. (b), black line shows garnet from sample Bt10/16ko with fractionated REE pattern, dashed line shows garnet from sample Bt 1/16 with low REE contents typical of exsolution garnets.

2013) showed that metasomatic enrichment of minerals is not necessarily related to the appearance of modal phlogopite, which is either absent or forms interstitial submicron phases (Agashev et al., 2013). In addition, so-called "melt" metasomatism occurred at higher temperatures. According to data presented in (Griffin et al., 1999b; Shchukina et al., 2017), the contents of trace elements, in particular, Zr, Y, and Ti, reflect specifics of garnet formation and bear signs of both partial melting and metasomatic enrichment of parental mantle rocks. A large amount of new geochemical data collected during the past decade showed that garnets with clear signs of metasomaic enrichment, in particular, with clearly expressed sinusoidal REE distribution pattern, fall in the field of depleted garnets according to classification (Griffin et al., 1999b). Half of lherzolitic garnets from sheared peridotites of the Udachnaya pipe (Agashev et al., 2013), i.e., rocks that were unambiguously subjected to intense metasomatism, and harzburgitic garnets from this pipe, which experienced carbonatite metasomatism, also fall in the field of depleted garnets according to classification (Griffin et al., 1999b). The compositional field of garnets from depleted rocks, which show geochemical signs of partial melting and could represent a residue after primitive mantle melting, was distinguished for the first time in (Shchukin at al., 2015). This field only partially overlaps the depleted garnet field distinguished by (Griffin, 1999b). Therefore, to characterize the compositional modification of garnet by metasomatic agents, we used classification proposed in (Shchukina et al., 2017; Agashev et al., 2018).

In terms of Zr–Y relations, all garnets in the xenoliths of the Nakyn kimberlite field correspond to metasomatized peridotites according to classification (Griffin, 1999b), except for one sample falling in the field of garnets from depleted mantle peridotites (Fig. 6). The majority of type 1 garnets fall in the field of garnets enriched by carbonatite/fluid metasomatism. The same field comprises harzburgitic garnet of diamond association ascribed to type 2 based on the REE distribution pattern. The type 1 garnets were

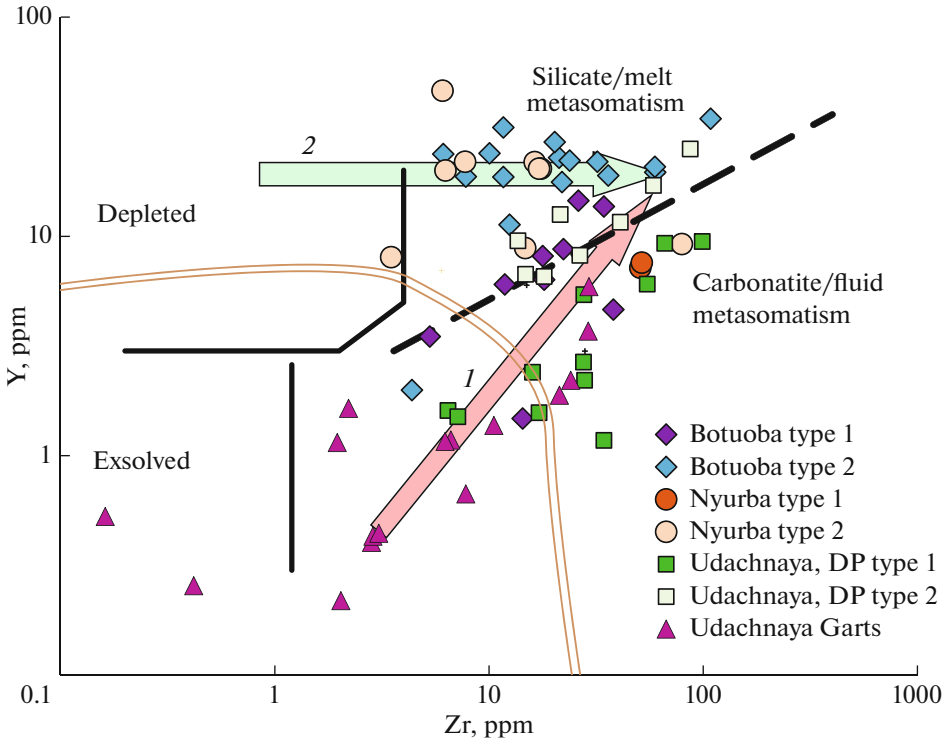

Fig. 6. Y–Zr diagram (modified after (Griffin et al., 1999b)) for garnets from peridotites of the Nakyn field compared to the garnets from peridotites of the Udachnaya pipe (Agashev et al., 2013; Pokhilenko et al., 2015). Compositional fields of garnets and types of metasomatism according to (Agashev et al., 2018). Double line distinguishes the field of garnets from depleted mantle rocks according to (Griffin et al., 1999b). (*1*) trend of garnets subjected to carbonatite (fluid) metasomatism; (*2*) trend of garnet subjected to silicate (melt) metasomatism.

likely formed in two stages. The first stage was responsible for the crystallization of harzburgitic garnets via reaction *Opx* + *Sp* = *Ol* + *Grt* (MacGregor, 1964). The appearance of forsterite association with garnet, orthopyroxene, and spinel is caused by the transition from spinel to garnet peridotites. It was shown that this reaction is assisted by high LREE/HREE fluid (Agashev et al., 2013; Chepurov et al., 2019). In the MgO–Al_2O_3–SiO_2 system, this reaction is monovariant. It was shown that the field of spinel-bearing association in the CaO–MgO–Al_2O_3–Cr_2O_3–SiO_2 system is displaced in the high-pressure region proportional to the bulk chromium content (MacGregor, 1970). In the quaternary Cr-bearing system, the equilibrium curve with increasing the number of degrees of freedom is transformed into the four-phase field *Grt* + *Ol* + *Opx* + *Sp* (Turkin and Sobolev, 2009).

Continuing supply and fractional crystallization of metasomatic agent with formation of garnet and clinopyroxene led to the enrichment of harzburgitic garnets in Ca, Y, and HREE (trend *1* in Fig. 6) and finally to the transition of harzburgite into lherzolite. Two type 1 garnets from the Botuoba pipe have the elevated Y content (>12 ppm), which could be caused by subsequent overprinting by silicate metasomatism. Type 2 garnets were likely subjected to the silicate metasomatism and their compositions fall in the corresponding region in the Zr–Y diagram. Silicate metasomatism that produced REE patterns of type 2 garnets likely developed after garnets of initially different compositions: garnets from depleted rocks (trend *2* in Fig. 6) or type 1 garnets that previously experienced carbonatite metasomatism (trend *1*). The formation of harzburgitic garnets as well as stages and sequence of their evolution along trend *1* are well consistent with a model of metasomatic evolution of peridotite garnets proposed in (Pokhilenko et al., 2015).

The formation of garnets and clinopyroxenes in sheared peridotites of the Udachnaya pipe (Agashev et al., 2010) is also thought to be related to the influence of carbonatite and silicate melts. Thereby, the influence of carbonatite melt is considered as the earliest stage of mantle metasomatism (Zedgenizov et al., 2020), which caused the formation of garnets with a clear sinusoidal REE pattern. According to inclusion data (Stachel and Harris, 2008), these garnets most frequently associate with diamond (Stachel and Harris, 2008). Therefore, garnets with such REE patterns could be ascribed to a group of potentially diamondiferous peridotites. Lherzolitic garnets with weakly expressed sinusoidal REE patterns also occur as inclusions in kimberlite diamonds worldwide (Stachel et al., 2004). It is more likely that garnets with less expressed

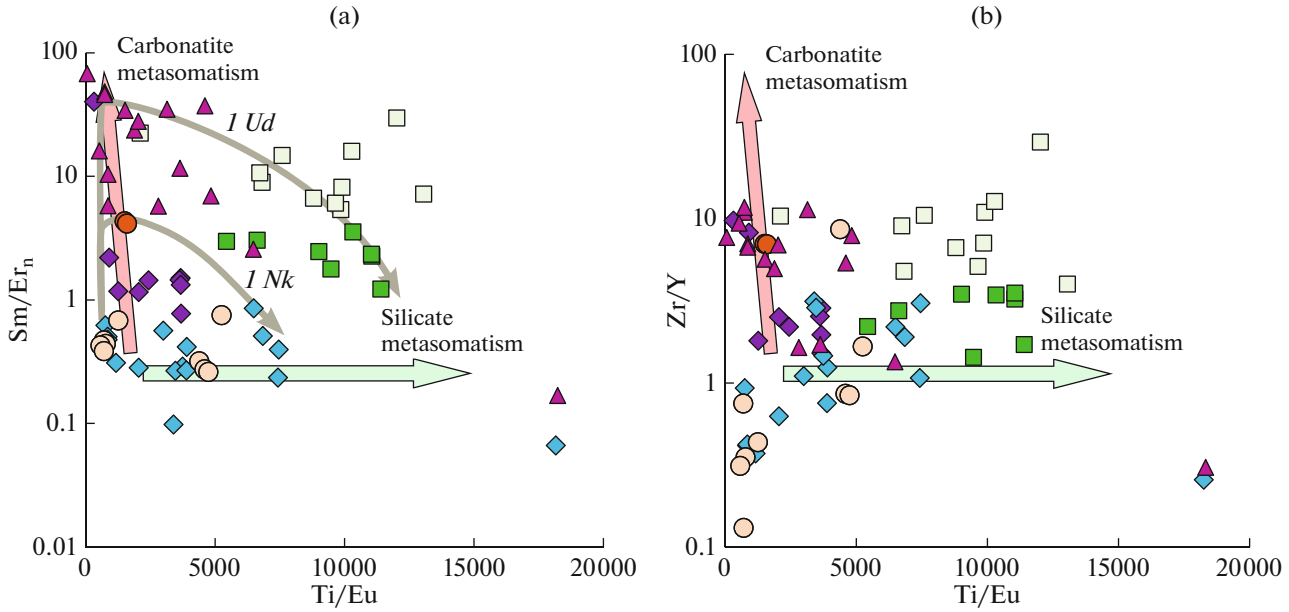

Fig. 7. Eidences for metasomatic reworking of the studied garnets in the $(Sm/Er)_n$–Ti/Eu (a) and Zr/Y–Ti/Eu (b) diagrams. Shown are evolutionary paths of garnets from harzburgitic through lherzolitic with sinusoidal REE distribution pattern to normal lherzolitic garnets from peridotites of the Udachnaya pipe (trend *1 Ud*) and Nakyn field (trend *1 Nk*). Symbols are shown in Fig. 6.

sinusoidal patterns experienced stronger metasomatic alteration, which is expressed in their enrichment in HREE and depletion in LREE.

Lherzolitic garnets with a normal REE distribution pattern are usually not associated with diamonds (except for Birim area, Stachel et al., 2004) because they are in equilibrium with silicate metasomatic agent, which is unfavorable for diamond survival (Agashev et al., 2018b). The metasomatic agent likely becomes high-temperature and acquires high Fe^{3+}/Fe_{tot} (Shchukina et al., 2015). According to the experimental data, such melts efficiently oxidize diamond (Rohrbach and Schmidt, 2011; Bataleva et al., 2012) and could cause a complete diamond annihilation when entering the lithospheric mantle.

Trace-element ratios can be used to estimate the intensity of metasomatic reworking of lithosphere mantle beneath the Nakyn kimberlite field (Figs. 7a, 7b). Figure 7a shows the evolutionary path of garnet from harzburgitic through lherzolitic with sinusoidal REE pattern to the normal lherzolitic garnets for the peridotites of the Udachnaya pipe (trend *1 Ud)* and Nakyn (trend *1 Nk*) fields. All garnets from the Nakyn field, except for one sample, have Ti/Eu ratio below 8000, which suggests a moderate reworking of lithospheric mantle peridotites by silicate melts compared to the mantle in the Udachnaya pipe area. Moreover, some samples with type 2 lherzolitic garnets have low Ti/Eu (500–1300) and Zr/Y (0.1–0.7) ratios, which indicates a weak metasomatic impact. These garnets in the Zr–Y diagram (Fig. 6) fall closely to the depleted garnet field and were likely formed after residual garnets in the course of the insignificant interaction with silicate metasomatic agents. The type 1 garnets from both pipes have elevated $(Sm/Er)_n$ and Zr/Y ratios, which serve as evidence for the carbonatite/fluid metasomatism. The intensity of this type of metasomatism in the garnets of the Nakyn field is also less expressed than in the garnets from the Udachnaya pipe. In particular, only five samples have the well expressed sinusoidal REE distribution pattern ($(Sm/Er)_n > 2$) or $Zr/Y > 5$, whereas the composition of other garnets of this type marks the final stage of carbonatite metasomatism by already strongly fractionated metasomatic agent depleted in MREE and enriched in HREE and Y. Obtained results indicate a moderate metasomatic reworking of lithospheric mantle beneath the Nakyn kimberlite field, which is consistent with a weak previously established incompatible element enrichment of the Nakyn kimberlites compared to the typical kimberlites (Agashev et al., 2001).

CONCLUSIONS

In terms of chemical composition of relict garnets, serpentinized peridotite xenoliths from the Botuoba and Nyurba pipes are classified as lherzolites (30 samples), harzburgites (6 samples), and websterites (1 sample). In terms of trace and rare-earth element composition and shape of chondrite-normalized REE patterns, the garnets are divided into two types. The first type is characterized by the sinusoidal REE pattern ($(Sm/Er)_n > 1$), which is more expressed in the harzburgitic garnets and less expressed in the lherzolitic garnets. The second type of garnets has the normal

REE distribution and, respectively, $(Sm/Er)_n < 1$. It is represented by lherzolitic garnets, one harzburgitic garnet, and one websteritic garnet. In terms of trace-element relations, all garnets from xenoliths of the Nakyn kimberlite field correspond to metasomatized peridotites (Agashev et al., 2018), except for one sample falling in the field of depleted garnets. It is suggested that the formation of type 1 garnets was assisted by carbonatite/fluid metasomatism, while type 2 garnets were formed in the presence of silicate metasomatic agents.

The type 1 garnets were formed in two stages. The first stage produced harzburgitic garnets through the transition from spinel to garnet peridotites. It was shown that this reaction in the $MgO–Al_2O_3–SiO_2$ system can be written as *Opx* + *Sp* = *Ol* + *Grt* and proceeds in the presence of high LREE/HREE fluid. The impact of carbonatite metasomatism on harzburgitic garnets at the second stage led to the formation of lherzolitic garnets with sinusoidal REE pattern. Metasomatism that was responsible for the formation of REE patterns of type 2 garnets was developed after garnets of different initial compositions: (1) depleted garnets, (2) type 1 garnets previously subjected to carbonatite metasomatism. Obtained results however, indicate a moderate metasomatic reworking of lithosphere mantle beneath the Nakyn kimberlite field compared to the typical kimberlites and their high diamond grade.

FUNDING

Sampling, sample preparation procedure, petrographic description, and analysis of trace element composition were financially supported by the Russian Science Foundation (16-17-10067). The determination of garnet composition was supported by the Russian Foundation for Basic Research (18-05-70064). All authors took part in the interpretation of results and preparation of the manuscript.

REFERENCES

A. M. Agashev, "Geochemistry of garnet megacrysts from the Mir kimberlite pipe (Yakutia) and the nature of protokimberlite melts," Dokl. Earth Sci. **486** (5), 675–678 (2019).

A. M. Agashev, Yu. Orikhashi, T. Watanabe, N. P. Pokhilenko, and V. P. Serenko, "Isotope-geochemical characteristics of kimberlites of the Siberian Platform: the problem of their origin," Geol. Geofiz. **41** (1), 90–99 (2000).

A. Agashev, T. Watanabe, D. Bydaev, N. Pokhilenko, A. Fomin, K. Maehara, and J. Maeda, "Geochemistry of kimberlites from the Nakyn field, Siberia: evidence for unique source composition," Geology. **29** (3), 267–270 (2001).

A. M. Agashev, N. P. Pokhilenko, A. V. Tolstov, V. G. Polyanichko, V. G. Mal'kovets, and N. V. Sobolev, "New age data on kimberlites from the Yakutian diamondiferous province," Dokl. Earth Sci. **399** (1), 1142–1145 (2004).

A. M. Agashev, N. P. Pokhilenko, Yu. V. Cherepanova, and A. V. Golovin, "Geochemical evolution of rocks at the base of the lithospheric mantle: evidence from study of xenoliths of deformed peridotites from kimberlite of the Udachnaya Pipe," Dokl. Earth Sci. **432** (4), 746–749 (2010).

A. Agashev, D. Ionov, N. Pokhilenko, A. Golovin, Y. Cherepanova, and I. Sharygin, "Metasomatism in lithospheric mantle roots: constraints from whole–rock and mineral chemical composition of deformed peridotite xenoliths from kimberlite pipe Udachnaya," Lithos **160**, 201–215 (2013).

A. M. Agashev, I. V. Serov, A. V. Tolstov, E. V. Shchukina, A. L. Ragozin, and N. P. Pokhilenko, "New genetic classification of garnets of lithospheric mantle," *Efficiency of Prospecting Works for Diamond: Prediction–Resource, Methodical, and Innovation–Ways of its Icrease* (NIGP AL Alrosa, Mirny, 2018a), pp. 39–341 [in Russian].

A. M. Agashev, S. I. Nakai, I. V. Serov, A. V. Tolstov, K. V. Garanin, and O. E. Kovalchuk, "Geochemistry and origin of the Mirny field kimberlites, Siberia," Mineral. Petrol. **112** (2), 597–608 (2018b).

A. M. Agashev, M. V. Chervyakovskaya, I. V. Serov, A. V. Tolstov, E. V. Agasheva, and S. L. Votyakov, "Source rejuvenation vs. re–heating: constraints on Siberian kimberlite origin from U/Pb and Lu/Hf isotope compositions and geochemistry of mantle zircons," Lithos. **364–365**, 105508 (2020).

T. Andersen and E.-R. Neumann, "Fluid inclusions in mantle xenoliths," Lithos. **55** (1), 301–320 (2001).

N. Arndt, N. Coltice, H. Helmstaedt, and M. Gregoire, "Origin of Archean subcontinental lithospheric mantle: some petrological constraints," Lithos **109** (1–2), 61–71 (2009).

Y. V. Bataleva, Y. N. Palyanov, A. G. Sokol, Y. M. Borzdov, and G. A. Palyanova, "Conditions for the origin of oxidized carbonate–silicate melts: Implications for mantle metasomatism and diamond formation," Lithos **128–131**, 113–125 (2012).

D. R. Bell, M. Gregoire, T. Grove, N. Chatterjee, R. Carlson, and P. Buseck, "Silica and volatile-element metasomatism of Archean mantle: a xenolith–scale example from the Kaapvaal Craton," Contrib. Mineral. Petrol. **150** (3), 251 (2005).

Y. Bussweiler, D. G. Pearson, T. Stachel, and B. A. Kjarsgaard, "Cr–rich megacrysts of clinopyroxene and garnet from Lac de Gras kimberlites, Slave Craton, Canada-implications for the origin of clinopyroxene and garnet in cratonic lherzolites," Mineral. Petrol. **112** (2), 583–596 (2018).

D. Carswell "Mantle derived lherzolite nodules associated with kimberlite, carbonatite and basalt magmatism: a review," Lithos. **13**(2), 121–138 (1980).

A. A. Chepurov, S. W. Faryad, A. M. Agashev, L. Strnad, R. Jedlicka, A. I. Turkin, M. Mihaljevic, and V. V. Lin, "Experimental crystallization of a subcalcic Cr-rich pyrope in the presence of REE-bearing carbonatite," Chem. Geol. **509**, 103–114 (2019).

L. S. Doucet, A. H. Peslier, D. A. Ionov, A. D. Brandon, A. V. Golovin, and I. V. Ashchepkov, "High water contents in the Siberian cratonic mantle: an FTIR study of

Udachnaya peridotite xenoliths," *AGUFM*, T23A–2563 (2013).

D. W. Eaton, F. Darbyshire, R. L. Evans, H. Grütter, A. G. Jones, and X. Yuan, "The elusive lithosphere–asthenosphere boundary (LAB) beneath cratons," Lithos **109** (1), 1–22 (2009).

M. Grégoire, D. Bell, and A. Le Roex, "Garnet lherzolites from the Kaapvaal Craton (South Africa): trace element evidence for a metasomatic history," J. Petrol. **44** (4), 629–657 (2003).

M. Grégoire, S. Jégo, R. Maury, M. Polvé, B. Payot, R. Tamayo. Jr., and G. Yumul, Jr., "Metasomatic interactions between slab–derived melts and depleted mantle: Insights from xenoliths within Monglo adakite (Luzon arc, Philippines)," Lithos **103** (3–4), 415–430 (2008).

W. Griffin, N. Fisher, J. Friedman, C. Ryan, and S. O'Reilly, "Cr-pyrope garnets in the lithospheric mantle. I. Compositional systematics and relations to tectonic setting," J. Petrol. **40** (5), 679–704 (1999a).

W. L. Griffin, S. R. Shee, C. G. Ryan, T. T. Win, and B. A. Wyatt, "Harzburgite to lherzolite and back again: metasomatic processes in ultramafic xenoliths from the Wesselton kimberlite, Kimberley, South Africa," Contrib. Mineral. Petrol. **134** (2), 232–250 (1999b).

B. Harte, "Mantle peridotites and processes–the kimberlite sample," *Continental Basalts and Mantle Xenoliths,* Ed. by C. Hawkesworth and M. J. Norry (Shiva, Nantwich, 1983), pp. 46–91.

C. Hawkesworth, A. Erlank, P. Kempton, and F. Waters, "Mantle metasomatism: isotope and trace–element trends in xenoliths from Kimberley, South Africa," Chem. Geol. **85**(1–2), 19–34 (1990).

K. Hidas, T. Guzmics, C. Szabó, I. Kovács, R. J. Bodnar, Z. Zajacz, Z. Nédli, L. Vaccari, and A. Perucchi, "Coexisting silicate melt inclusions and H_2O-bearing, CO_2-rich fluid inclusions in mantle peridotite xenoliths from the Carpathian–Pannonian region (central Hungary)," Chem. Geol. **274** (1–2), 1–18 (2010).

K. Hoal, B. Hoal, A. Erlank, and N. Shimizu, "Metasomatism of the mantle lithosphere recorded by rare earth elements in garnets," Earth Planet. Sci. Lett. **126** (4), 303–313 (1994).

G. H. Howarth, P. H. Barry, J. F. Pernet–Fisher, I. P. Baziotis, N. P. Pokhilenko, L. N. Pokhilenko, R. J. Bodnar, L. A. Taylor, and A. M. Agashev, "Superplume metasomatism: evidence from Siberian mantle xenoliths," Lithos **184**, 209–224 (2014).

D. A. Ionov, L. S. Doucet, and I. V. Ashchepkov, "Composition of the lithospheric mantle in the Siberian craton: new constraints from fresh peridotites in the Udachnaya–East kimberlite," J. Petrol. **51** (11), 2177–2210 (2010).

D. A. Ionov, F. Bigot, and R. Braga, "The provenance of the lithospheric mantle in continental collision zones: petrology and geochemistry of peridotites in the Ulten–Nonsberg Zone (Eastern Alps)," J. Petrol. **58 (7)**, 1451–1472 (2017).

D. A. Ionov, L. S. Doucet, P. A. P. von Strandmann, A. V. Golovin, A. V. Korsakov, "Links between deformation, chemical enrichments and Li–isotope compositions in the lithospheric mantle of the central Siberian craton," Chem. Geol. **475**, 105–121 (2017).

A. V. Kargin, L. V. Sazonova, A. A. Nosova, N. M. Lebedeva, V. V. Tretyachenko, and A. Abersteiner, "Cr–rich clinopyroxene megacrysts from the Grib kimberlite, Arkhangelsk province, Russia: relation to clinopyroxene–phlogopite xenoliths and evidence for mantle metasomatism by kimberlite melts," Lithos **292–293**, 34–48 (2017).

A. I. Kiselev, V. V. Yarmolyuk, A. V. Ivanov, and K. N. Egorov, "Middle Paleozoic basaltic and kimberlitic magmatism in the northwestern shoulder of the Vilyui Rift, Siberia: relations in space and time," Russ. Geol. Geophys. **55** (2), 144–152 (2014).

O. Klein–BenDavid, E. S. Izraeli, E. Hauri, and O. Navon, "Mantle fluid evolution—a tale of one diamond," Lithos **77** (1–4), 243–253 (2004).

K. M. Konstantinov, A. A. Yakovlev, T. A. Antonova, I. K. Konstantinov, Sh. Z. Ibragimov, and E. V. Artemova, "Petro- and paleomagnetic characteristics of the structural–material complexes of the diamond mining of the Nyurbinskaya pipe (Middle Markha district, West Yakutia)," Geodynam. Tectophys. **8** (1), 135–169 (2017).

J. M. Koornneef, M. U. Gress, I. L. Chinn, H. A. Jelsma, J. W. Harris, and G. R. Davies, "Archaean and Proterozoic diamond growth from contrasting styles of large–scale magmatism," Nat. Commun. **8** (1), 1–8 (2017).

M. Kopylova, J. Russell, and H. Cookenboo, "Petrology of peridotite and pyroxenite xenoliths from the Jericho kimberlite: implications for the thermal state of the mantle beneath the Slave craton, northern Canada," J. Petrol. **40** (1), 79–104 (1999).

M. Kopylova, J. Russell, C. Stanley, and H. Cookenboo, "Garnet from Cr–and Ca–saturated mantle: implications for diamond exploration," J. Geochem. Explor. **68** (3), 183–199(2000).

M. Y. Koreshkova, H. Downes, L. K. Levsky, and N. V. Vladykin, "Petrology and geochemistry of granulite xenoliths from Udachnaya and Komsomolskaya kimberlite pipes, Siberia," J. Petrol. **52**, 1857–1885 (2011).

V. P. Kornilova, A. S. Fomin, and A. M. Zaitsev, "New type of diamondiferous kimberlite rocks at the Siberian Platform," Regional. Geol. Metallogen. **13–14**, 105–117 (2001).

Yu. G. Lavrent'ev, N. S. Karmanov, and L. V. Usova, "Electron probe microanalysis of minerals: mcroanalyzer or scanning electron microscope?" Russ. Geol. Geophys. **56** (8), 1154–1161 (2015).

I. D. MacGregor, "The reaction 4 enstatite + spinel = forsterit e+ pyrope," Carnegie Inst Wash Ybk. **63**, 156–157 (1964).

I. D. Macgregor, "The effect of CaO, Cr_2O_3, Fe_2O_3 and Al_2O_3 on the stability of spinel and garnet peridotites," Phys. Earth Planet. Int. **3**, 372–377 (1970).

V. Malkovets, D. Zedgenizov, W. Griffin, A. Dak, S. O'Reilly, N. Pokhilenko, and S. Mityukhin, "Diamondiferous microxenoliths and xenocrysts from the Nyurbinskaya kimberlite pipe, Yakutia," *9th International Kimberlite Conference Extended Abstract*, No. 9IKC–A–00224 (2008).

W. F. McDonough and S.-S. Sun, "The composition of the Earth," Chem. Geol. **120** (3–4), 223–253 (1995).

R. H. Mitchell, A. Giuliani, and H. O'Brien, "What is a kimberlite? Petrology and mineralogy of hypabyssal kimberlites," Elements **15**(6), 381–386 (2019).

D. G. Pearson, D. Canil, and S. B. Shirey, "Mantle samples included in volcanic rocks: xenoliths and diamonds," In *Treatise on Geochemistry,* Ed. by R. W. Carlson (Elsevier, 2003), pp. 171–275.

D. G. Pearson, J. Woodhead, and P. E. Janney, "Kimberlites as geochemical probes of Earth's mantle," Elements **15** (6), 387–392 (2019).

N. P. Pokhilenko, N. V. Sobolev, S. D. Chernyi, and Yu. T. Yanygin, "Pyropes and chromites from kimberlites in the Nakyn Field (Yakutia) and Snipe Lake district (Slave River Region, Canada): evidence for anomalous structure of the lithosphere," Dokl. Earth Sci. **372** (3), 638–642 (2000).

N. P. Pokhilenko, A. M. Agashev, K. D. Litasov, and L. N. Pokhilenko, "Carbonatite metasomatism of peridotite lithospheric mantle: implications for diamond formation and carbonatite–kimberlite magmatism," Russ. Geol. Geophys. **56** (1–2), 280–295 (2015).

A. Rohrbach and M. W. Schmidt, "Redox freezing and melting in the Earth's deep mantle resulting from carbon–iron redox coupling," Nature **472** (7342), 209–212 (2011).

O. M. Rosen, L. K. Levskii, D. Z. Zhuravlev, A. Ya. Rotman, Z. V. Spetsius, A. F. Makeev, N. N. Zinchuk, A. V. Manakov, and V. P. Serenko, "Paleoproterozoic accretion in the northeast Siberian Craton: isotopic dating of the Anabar collision system," Stratigraphy. Geol. Correlation **14** (6), 581–601 (2006).

R. L. Rudnick and A. A. Nyblade, "The thickness and heat production of Archean lithosphere: constraints from xenolith thermobarometry and surface heat flow," In *Mantle Petrology: Field Observations and High Pressure Experimentation: a Tribute to Francis R.(Joe) Boyd,* Ed. by Y. Fei, C. M. Bertka, and B. O. Mysen, Geochem. Soc. Spec. Publ. **6**, 3–12 (1999).

V. Shatsky, A. Ragozin, D. Zedgenizov, and S. Mityukhin, "Evidence for multistage evolution in a xenolith of diamond–bearing eclogite from the Udachnaya kimberlite pipe," Lithos **105** (3–4), 289–300 (2008).

E. V. Shchukina. A. M. Agashev, S. I. Kostrovitskii, and N. P. Pokhilenko, "Metasomatic events in the lithospheric mantle beneath the V. Grib kimberlite pipe (Arkhangelsk diamondiferous province, Russia)," Russ. Geol. Geophys. **56** (12), 1701–1716 (2015).

E. V. Shchukina, A. M. Agashev, and N. P. Pokhilenko, "Metasomatic origin of garnet xenocrysts from the V. Grib kimberlite pipe, Arkhangelsk region, NW Russia," Geosci. Front. **8** (4), 641–651 (2017).

E. V. Shchukina, A. M. Agashev, and V. S. Shchukin, "Diamond-bearing root beneath the northern East European Platform (Arkhangelsk Region, Russia): evidence from Cr–pyrope trace–element geochemistry," Minerals **9** (5), 261 (2019).

N. V. Sobolev, *Mantle Inclusions in Kimberlites and Problem of Upper Mantle Composition* (Nauka, Novosibirsk, 1974) [in Russian].

N. V. Sobolev, Y.G. Lavrent'ev, N. P. Pokhilenko, and L. V. Usova, "Chrome–rich garnets from the kimberlites of Yakutia and their parageneses," Contrib. Mineral. Petrol. **40** (1), 39–52 (1973).

Z. V. Spetsius, A. S. Ivanov, and S. I. Mityukhin, "Diamondiferous xenoliths and megacrysts from the Nyurbinskaya kimberlite pipe (Nakynsky Field, Yakutia)," Dokl. Earth Sci. **408** (6), 779–783 (2006).

Z. V. Spetsius, L. A. Taylor, J. W. Valley, M. T. Deangelis, M. Spicuzza, A. S. Ivanov, and V. I. Banzeruk, "Diamondiferous xenoliths from crustal subduction: garnet oxygen isotopes from the Nyurbinskaya pipe, Yakutia," Eur. J. Mineral. **20** (3), 375–385 (2008).

T. Stachel and J. W. Harris, "The origin of cratonic diamonds–constraints from mineral inclusions," Ore Geol. Rev. **34** (1–2), 5–32 (2008).

T. Stachel, S. Aulbach, G. P. Brey, J. W. Harris, I. Leost, R. Tappert, K. F. Viljoen, "The trace element composition of silicate inclusions in diamonds: a review," Lithos. **77 (1–4)**, 1–19 (2004).

J. Sun, C. Liu, S. Tappe, S. I. Kostrovitsky, F. Wu, D. Yakovlev, Y. Yang, and J. Yang, "Repeated kimberlite magmatism beneath Yakutia and its relationship to Siberian flood volcanism: Insights fromin situ U–Pb and Sr–Nd perovskite isotope analysis," Earth Planet. Sci. Lett. **404**, 283–295 (2014).

L. A. Taylor and M. Anand, "Diamonds: time capsules from the Siberian mantle," Chem. Erde–Geochemistry. **64** (1), 1–74 (2004).

A. V. Tolstov, V. A. Minin, L. G. Kuznetsov, and A. N. Razumov, "A new body of highly diamonidiferous kimberltes in the Nakyn field of the Yakutian kimberlite province," Russ. Geol. Geophys. **50** (3), 162–173 (2009).

E. Tomlinson, A. Jones, and J. Harris, "Co–existing fluid and silicate inclusions in mantle diamond," Earth Planet. Sci. Lett. **250** (3–4), 581–59 (2006).

M. D. Tomshin, A. S. Fomin, V. P. Kornilova, S. D. Chernyi, and Yu. T. Yanygin, "Magmatic rocks of the Nakyn kimberlite field, Yakutian province," Russ. Geol. Geophys. **39**(12), 1693–1703 (1998).

A. I. Turkin and N. V. Sobolev, "Pyrope–knorringite garnets: overview of experimental data and natural parageneses," Russ. Geol. Geophys. **50** (12), 1169–1182 (2009).

D. A. Zedgenizov, S. Yu. Skuzovatov, W. L. Griffin, A. L. Ragozin, and V. V. Kalinina, "Diamond-forming HDFs tracking episodic mantle metasomatism beneath Nyurbinskaya kimberlite pipe (Siberian craton)," Contrib. Mineral. Petrol. **175** (11), 1–21 (2020).

Translated by M. Bogina